Effects of Approximation and Close-Fitting Technique of Corona Model on Neon Soft X-Ray Emission in 3-kJ Plasma Focus

Article *in* IEEE Transactions on Plasma Science · July 2015

DOI: 10.1109/TPS.2015.2433301

6 authors, including:

Saiful Najmee Mohamad

Universiti Sains Malaysia

Kashif Chaudhary

Universiti Teknologi Malaysia

Sor Heoh Saw

Nilai University, Negeri Sembilan, Malaysia

Jalil Ali

Universiti Teknologi Malaysia

Effects of Approximation and Close-Fitting Technique of Corona Model on Neon Soft X-Ray Emission in 3-kJ Plasma Focus

Natashah Abd Rashid, Saiful Najmee Mohamad, Kashif Tufail Chaudhary, Sing Lee, Sor Heoh Saw, and Jalil Ali

***Abstract*— In plasma focus (PF), the thermodynamic parameters such as ion fraction α, effective ionic charge number Z_{eff}, and effective specific heat ratio γ at different temperatures may be calculated by corona model (CM). In the Lee model code, the neon Z_{eff} and γ are stored in subroutines using convenient tables and polynomials derived from the CM (we call this approach approximated CM). In this paper, the thermodynamic parameters of the CM are close fitted to the data, thus replacing the approximate CM data with a more accurate close-fitting CM (CFCM). The comparisons of the Lee model code using the approximated CM and CFCM subroutines are conducted, with the main emphasis on optimum neon soft X-ray (SXR) emission and their properties. The suitable focus pinch temperature window of 200–500 eV is applied to generate the optimum neon SXR yield (Y_{sxr}). The optimum neon Y_{sxr} is found to be 3.19 and 3.49 J at the optimum pressure $P_0 = 3.1$ torr with approximated CM and CFCM subroutines, respectively. A high optimum value of SXR yield is obtained using CFCM subroutines in the Lee model, which is nearer to the experimental value compared with the approximated CM subroutines. The use of CFCM in the Lee model contributes to better estimation for further numerical experiment studies and gives confidence that the model is sufficiently realistic in describing the PF dynamics and SXR emission.**

***Index Terms*— γ, approximated corona model (approximated CM), close-fitting of corona model (CFCM), corona model (CM), ionic charge number, soft X-ray (SXR), specific heat ratio, Z_{eff} plasma focus (PF).**

I. Introduction

PLASMA focus (PF) machines operated in neon have been studied as intense sources of soft X-rays (SXRs) [1]–[3]. The dynamics of PF discharges are complicated, and the Lee model code provides a useful tool to conduct phenomenological scaling studies for any PF device from low energy to high energy [4]. The Lee model couples the electrical circuit with PF dynamics, thermodynamics, and radiation, enabling realistic simulation of all gross PF properties [5]–[7]. The code incorporates radiation mechanisms and uses the corona model (CM) for the calculation of thermodynamic data to input into the code.

CM computation [8] is utilized to calculate the ionization fractions at any high temperature. From these ionization fractions, the effective specific heat ratio γ and effective ionic charge number Z_{eff} are calculated as functions of temperature [6], [9]. In the Lee code, the Z_{eff} and γ are calculated from subroutines [10]–[12] using the approximated CM [5], [6], [13], [14] with approximated tables and polynomials.

In this paper, the Z_{eff} and γ are precisely and closely fitted to the Z_{eff} and γ data in the CM [we call this the close-fitting CM (CFCM) data]. From the numerical experiments [15], [16] it has been observed that the Lee model code not only computes the realistic focus dynamics but also gives absolute values of SXR yield (Y_{sxr}), which are consistent with experimental measurements. Therefore, the increased precision of CM data using CFCM used in the Lee model may develop more realistic computational results. We compare these approximated CM and CFCM cases to investigate the effect on the yields of SXR.

To characterize the PF device operated in neon, the Lee model code is configured for low-energy PF device: 3-kJ UNU/ICTP PFF. The neon ionization energy data are extracted from the National Institute of Standards and Technology (NIST) [9]. We then use the approximate CM and the CFCM to provide effective charge numbers and specific heat ratios for neon, which are fed, in turn, into the Lee model code version RADPF5.15de, in order to compare the difference in the results using the two different sets of thermodynamic data.

II. Calculations of Thermodynamic Neon Plasma Parameters

Based on the CM, the plasma equilibrium model [17] is used to calculate the ion fraction α, the effective ionic charge number Z_{eff}, the effective specific heat ratio γ, and X-ray emission of the plasma at different temperatures. Shan [10] has conducted a line-by-line computation using CM and determined the relative intensities of each of the four neon SXR lines (He- and H-like) as functions of temperature. From the ionization data computed from the CM, it is deduced that the plasma temperature range 200–500 eV [7] is suitable for optimum yield of neon Y_{sxr}. This is consistent with the observation that the electron temperature of X-ray radiative plasmas for neon is 250–500 eV [9] and that the average

Manuscript received January 19, 2014; revised August 6, 2014, September 21, 2014, and December 18, 2014; accepted May 6, 2015.

N. Abd Rashid, S. N. Mohamad, K. T. Chaudhary, and J. Ali are with the Institute of Advanced Photonic Science, Nanotechnology Research Alliance, Universiti Teknologi Malaysia, Johor Bahru 81310, Malaysia (e-mail: natashah.abdrashid@yahoo.com; naj_mohamad@yahoo.com; kashif.ali02@gmail.com; jalilali@utm.edu.my).

S. Lee is with INTI International University, Nilai 71800, Malaysia, also with the Institute for Plasma Focus Studies, Melbourne, VIC 3148, Australia, and also with the University of Malaya, Kuala Lumpur 50603, Malaysia (e-mail: leesing@optusnet.com.au).

S. H. Saw is with INTI International University, Nilai 71800, Malaysia, and also with the Institute for Plasma Focus Studies, Melbourne, VIC 3148, Australia (e-mail: sorheoh.saw@newinti.edu.my).

Digital Object Identifier 10.1109/TPS.2015.2433301

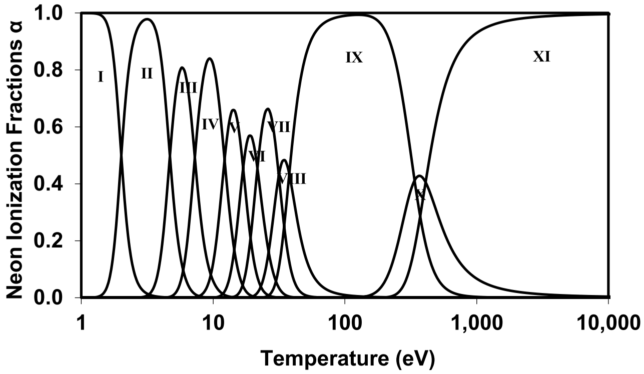

Fig. 1. Neon ion fraction at different temperatures, where IX indicates Ne+8 (calculated by CM).

electron temperature is ∼300 ± 50 eV, as has been experimentally measured in an efficient system [11]. The ion concentrations can also be identified [18] by solving the equations for ionization fraction α to calculate the X-ray emission or absorption from plasma.

The ionization fraction is defined as the fraction of plasma that is ionized up to the zth ionized state. It can be written as

$$\alpha_z = \frac{N_z}{N_i} \tag{1}$$

where N_z is the number of ions in the zth state and N_i is the total ion number densities in the plasma.

In this paper, the ionization fraction calculations as shown in (1) depend on the balance collision process [19] between the ionization coefficient evaluated from comparison with the Coulomb–Born approximation in [20] and the radiative recombination coefficient in [21]. The data of ionization potentials and X-ray emission spectrum of highly ionized neon plasma are taken from the NIST database [22].

Fig. 1 shows the ionization fraction in neon plasma. From Fig. 1, it is observed that the suitable temperature window to produce H-like and He-like ions in neon plasma (for SXR emissions) is between 200 and 500 eV [7], [11], [23], [24]. Based on the experimental results [10], [11], [25], the X-ray emissions from neon plasma are mainly H-like [Ly$_\alpha$ (1s-2p), Ne: 12.132 Å (1022 eV), Ly$_\beta$ (1s-3p), Ne: 10.240 Å (1211 eV)] and He-like [He$_\alpha$ (1s^2-1s2p), Ne: 13.447 Å (922 eV), He$_\beta$ (1s^2-1s3p), Ne: 11.544 Å (1074 eV)], which are suitable for neon SXR production.

The effective ion charge number Z_{eff} can be calculated by the relation [10]

$$Z_{\text{eff}} = \frac{\sum_{z=0}^{Z_n}(zN_z)}{\sum_{z=0}^{Z_n} N_z} = \frac{N_e}{N_i} \tag{2}$$

where N_e and N_i are the electron and ion number densities, respectively, and N_z is the number density of the ions in the zth ionic state.

The ionization and excitation processes play an important role for energy balance and compressibility of the plasma. These effects can be described by the effective specific heat ratio γ using the following equation [24]:

$$\frac{\gamma}{\gamma-1} \approx \frac{5}{2} + \frac{E_i}{kT_e(1+Z_{\text{eff}})} \tag{3}$$

where k is the Boltzmann constant, T_e is the electron temperature (in kelvin), and E_i is the ionization energy.

III. Close-Fitting Technique for Z_{eff} and γ Data

In the Lee model code, Z_{eff} and γ from the CM are stored in approximate tables and polynomials [5], [6], [13], [14]. This code with approximated CM has been utilized for PF numerical experiments to estimate SXR [6], [23], [26], [27].

For this paper, we consider two cases of approximated CM and CFCM subroutines in the Lee model. The ionic charge number Z_{eff} and specific heat ratio γ from the approximated CM and CFCM are investigated to observe their effects on the neon SXR yield.

The code of Z_{eff} and γ data is generated based on the close-fitting approach on the Z_{eff}, and γ curves are produced by the CM data. The Z_{eff} and γ data are first obtained by fitting them with sixth-degree polynomials as high degree order via basic fitting in Excel VBA. The Z_{eff} versus temperature of $\log_{10}$ T (in electronvolts) and γ versus temperature of $\log_{10}$ T (in electronvolts) are plotted. This series of data is then used to fit with the basic fitting in the MATLAB code with polynomial fitting up to 10th degree to increase the accuracy for achieving good fitting precision. The process is continued until the final values of Z_{eff} with the corresponded temperature are obtained. The whole procedure is then repeated for the γ versus temperature.

At the final stage of fitting process, the sequence continuity of the series close fitting of Z_{eff} versus temperature and γ versus temperature (CFCM) is compared with CM as shown in Fig. 2(a) and (b). It is clearly observed that the data of Z_{eff} versus temperature and γ versus temperature in CM are fitted more precisely by CFCM.

IV. Results on the Z_{eff} and γ Between Approximated CM and CFCM Data

The computed Z_{eff} and γ data with CFCM subroutines are then compared with approximated CM subroutines, as shown in Fig. 3(a) and (b), respectively. In Fig. 3(a), there is a big difference in the approximated data and the CFCM data in the temperature range 2–3 eV corresponding to the first two stages of ionization. Based on Fig. 1, the temperature range of characteristic neon SXR emission for He-like and H-like neon ions in neon plasma is estimated between 200 and 500 eV in the CM. The temperature range 118.98–151.85 eV corresponds to the 1s^2 close shell for the neon ions is obtained, as shown in Fig. 3(a). Therefore, the yield from X-ray line emissions is low in this temperature range from neon. It is also found that the neon atoms become fully ionized as the temperature reaches 1000 eV and onward.

Although Fig. 3(b) shows considerable differences in the approximate CM and CFCM data in the region temperature <3 eV, the data in this temperature region are never used in the code since the radial phase temperature is never below 5 eV. Hence, the inaccuracies observed in the approximated CM subroutines do not contribute to the results of the code. Differences less than 5% are also observed for γ values in the temperature range 40–500 eV in which

This article has been accepted for inclusion in a future issue of this journal. Content is final as presented, with the exception of pagination.

(a)

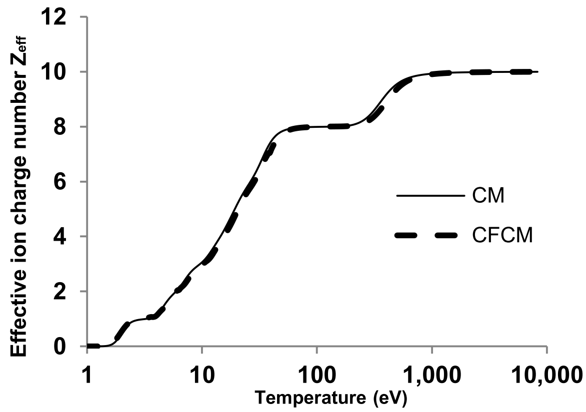

(b)

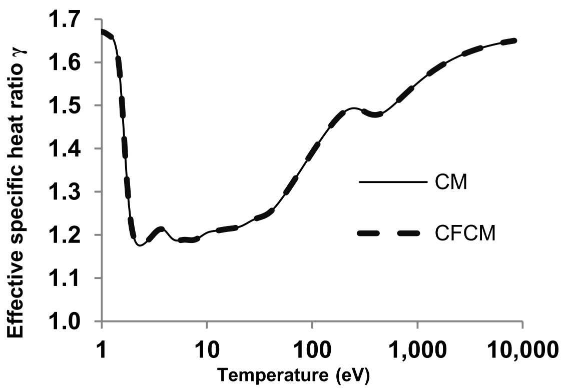

Fig. 2. Fitted CFCM curves with the CM data for (a) Z_{eff} versus temperature in electronvolts and (b) γ versus temperature in electronvolts.

He-like and H-like ions are produced. The higher value of γ with CFCM does affect the energy balance and plasma compressibility in the Lee model, resulting in a 10% change in the characteristic neon SXR yield in the example chosen for our comparison. Since the Z_{eff} and γ possess different values in the approximated CM and CFCM subroutines into the Lee model code, the neon SXR yield is also different for both cases.

The intensities of Lyman alpha (Ly_{α}) and helium alpha (He_{α}) lines are proportional to the H-like and He-like ion densities, respectively. Therefore, the power of line emissions can be calculated [5], [10], [11] for Ly_{α}, Ly_{β}, He_{α}, and He_{β} lines in neon as functions of photon energy ($h\upsilon$) using the following equations [11]:

$$P_{\text{Ly}\alpha(1s\text{-}2p)} = 2.13 \times 10^{-31} N_i^2 \frac{\alpha_9 Z_{\text{eff}}}{\sqrt{T}_{\text{eV}}} e^{\left(-\frac{h\upsilon_1}{T_{\text{eV}}}\right)} \quad (4)$$

$$P_{\text{Ly}\beta(1s\text{-}3p)} = 4.05 \times 10^{-32} N_i^2 \frac{\alpha_9 Z_{\text{eff}}}{\sqrt{T}_{\text{eV}}} e^{\left(-\frac{h\upsilon_2}{T_{\text{eV}}}\right)} \quad (5)$$

$$P_{\text{He}\alpha(1s^2\text{-}1s2p)} = 1.31 \times 10^{-31} N_i^2 \frac{\alpha_8 Z_{\text{eff}}}{\sqrt{T}_{\text{eV}}} e^{\left(-\frac{h\upsilon_3}{T_{\text{eV}}}\right)} \quad (6)$$

$$P_{\text{He}\beta(1s^2\text{-}1s3p)} = 3.30 \times 10^{-32} N_i^2 \frac{\alpha_8 Z_{\text{eff}}}{\sqrt{T}_{\text{eV}}} e^{\left(-\frac{h\upsilon_4}{T_{\text{eV}}}\right)} \quad (7)$$

(a)

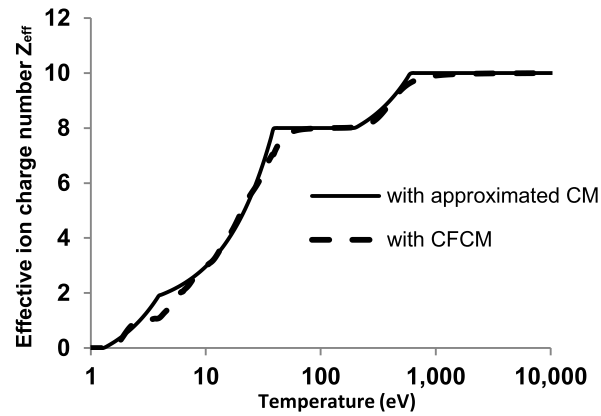

(b)

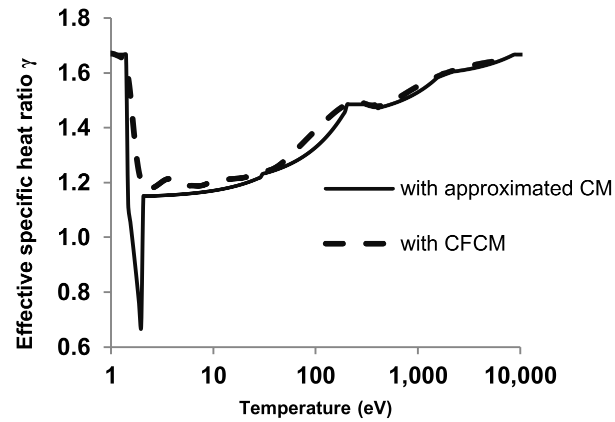

Fig. 3. Comparison between the approximated CM and CFCM subroutines of (a) Z_{eff} versus temperature and (b) γ versus temperature.

where $h\upsilon_1 = 1024.7$ eV, $h\upsilon_2 = 1214.1$ eV, $h\upsilon_3 = 924.5$ eV, and $h\upsilon_4 = 1196$ eV. From (4) to (7), it can be observed that the radiation power is proportional to the density squared N_{i}^2 ion fraction α and effective ionic charge number Z_{eff}. By selecting $N_i = 1$, the normalized emission intensity is calculated [5], [6], [11].

Referring to (4)–(7), the line emission intensities are calculated based on the ion fraction α and ionic charge number Z_{eff} in the CM, i.e., before the Z_{eff} data act as a subroutine into the Lee model code. Since this calculation is determined in the CM, no differences are observed for the line emission intensities for neon Ly and He lines although there are such approximated CM and CFCM subroutines incorporated in the Lee model code.

The calculated Ly and He emission intensities from one neon ion at unit density are shown in Fig. 4, which describes the correlation between the line emission intensity with the corresponding ions. The peaks of the Ly and He lines are located at the higher temperature side of the H-like and He-like ion distributions [5]. Specifically, Ly_{α} and He_{α} lines are the most intense characteristic emissions of neon plasma, whereas the other line radiations and the free-to-bound continuum

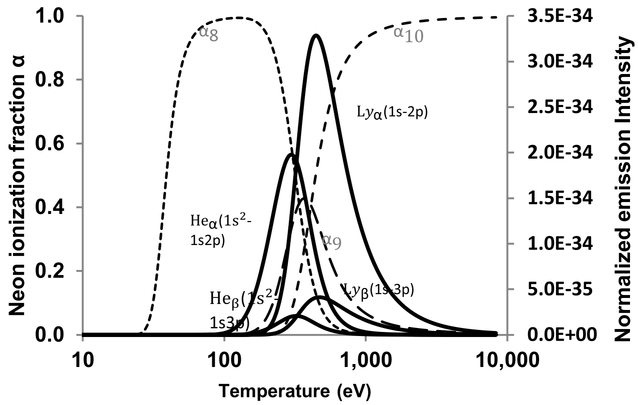

Fig. 4. Calculated X-ray line emission intensities from neon Ly and He lines versus temperature.

are weaker [11], [25]. The locations of the peaks give an estimation of the optimum temperatures for generating SXRs from neon plasma, i.e., 316 eV. As the line intensities are calculated based on the CM data, the range of pinch temperature of 200–500 eV is applied for CFCM and approximated CM.

V. Plasma Focus Numerical Experiments in Lee Model for Neon SXR

The properties of X-ray in the pinched plasma are mainly depending on the ionization states, plasma temperature, and density [10]. The focused plasma with an electron temperature of a few hundreds of electronvolts to kiloelectronvolts and high electron density is a copious source of X-rays. The PF emits soft thermal X-rays by three processes, namely, Bremsstrahlung (free–free transition) from the coulomb interactions between electrons and ions; recombination (free–bound transition), and de-excitation (bound–bound transition) [11], [28]. The first two processes give rise to the continuum of the X-ray spectrum, while the third process produces the line radiation or emission of the plasma. The relative strengths of the continuum and line emission [29] depend on how the plasma is generated [28]. For the plasma generated from a high-Z material, continuum emission dominates; while for a low-Z material, line emissions are stronger [10], [11].

In the pinch phase, the line radiation Q_L is calculated using the relation [1], [5]

$$\frac{dQ_L}{dt} = \frac{-4.6\times 10^{-31} n_i^2 Z_{\text{eff}} Z_n^4 (\pi r_p^2) Z_f}{T_e} \tag{8}$$

which is integrated over the pinch duration. The SXR energy generated within the plasma pinch depends on the number density n_i, effective charge number Z_{eff}, atomic number of gas Z_n, pinch radius r_p, pinch length z_f, plasma (pinch) temperature T_e, and pinch duration [15]. This generated energy is then reduced by the plasma self-absorption mainly on density and temperature; the reduced quantity of energy is then emitted as the Y_{sxr} [23].

Based on the CM, in the Lee model code, it is considered that the neon SXR yield (generation H-like and He-like ions) is equivalent to line radiation yield, i.e., $Y_{\text{sxr}} = Q_L$, in the following temperature range 200–500 eV. To run this code, the published experimental current waveform is chosen for fitting purposes to get the realistic measurement of computed (numerical experiment) results and actual experimental results. Then, the actual experimental results of Y_{sxr} are also used for the comparison with the computed results.

VI. Numerical Experimental Procedures Using RADPF5.15de

The Lee code is configured to work as any PF by inputting the bank parameters, the tube parameters, operational parameters, and the filled gas [5], [26], [30]. The standard practice is to fit the computed total current waveform to an experimentally measured total current waveform using four model parameters [1], [31], i.e., the mass swept-up factor (f_m) and the plasma current sheath factor (f_c) for the axial phase and radial mass swept-up and current factors f_{mr} and f_{cr} for the radial phase [5].

The exact time profile of the total current trace is governed by the bank parameters, focus tube geometry, and the operational parameters, [5] and also depends on f_m, f_c, and variation of these fractions through the axial and radial phases. These parameters determine the axial and radial dynamics, specifically the axial and radial speeds, which in turn affect the profile and magnitudes of the discharge current [5], [15]. Evidently, from the current trace, the information of axial and radial phase dynamics and the crucial energy transfer into the focus pinch are determined.

The detailed profile of the discharge current during the pinch phase reflects joule heating and radiative yields [30]. At the end of the pinch phase, the total current profile reflects the sudden transition of the current flow from a constricted pinch to a large column flow [32]. Thus, the electrodynamic, thermodynamic, and radiation processes in the various phases affect the discharge current. The discharge current waveform includes all the information of dynamic, electrodynamic, thermodynamic, and radiation processes that occur in the various phases of the PF. This explains the importance to fit the computed current trace to the measured current trace in the procedure adopted by the Lee model code [30].

VII. Lee Model Numerical Experiments for SXR Emission

The numerical experiments are performed with approximated CM subroutines in the Lee model code. In the next step, RADPF5.15de version of the Lee model code is modified by incorporating CFCM subroutines codes. By operating the Lee model with the CFCM and approximated CM, the numerical experiments are conducted for the standard 3-kJ UNU/ICTP PFF PF using the same bank, tube, and operational parameters as in [11]. The approach of CFCM is executed to observe the significance and effects on equilibrium properties of SXR emission.

The measured discharge current trace of the UNU/ICTP PFF filled with neon gas detected by Rogowski coil [11] is used to perform numerical experiments with the selected measured waveform of a shot at 3.0 torr neon [11]. The following configuration parameters [11] are used for the Lee model with the CFCM and approximated CM of neon.

This article has been accepted for inclusion in a future issue of this journal. Content is final as presented, with the exception of pagination.

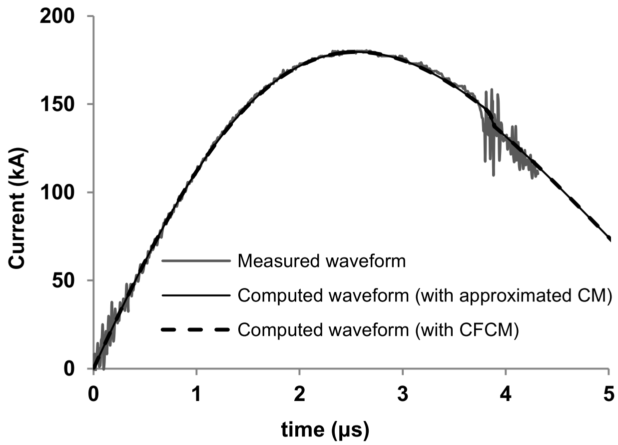

Fig. 5. Fitted model parameters of the total computed current waveform at 3.0 torr to those of the experimentally measured current waveform at the same 3.0 torr of neon with the CFCM and approximated CM.

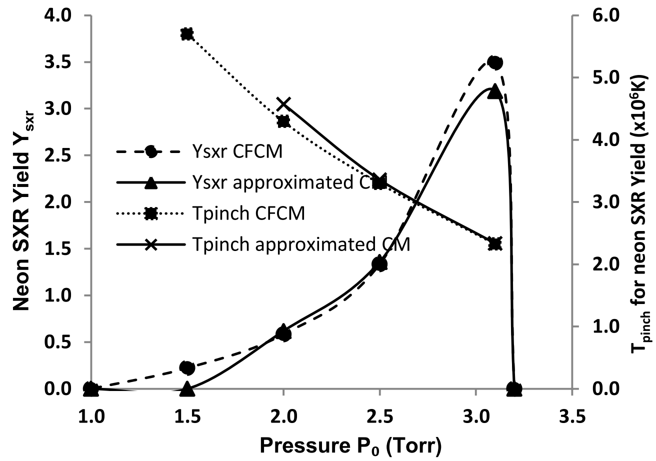

Fig. 6. Numerical experimental result of Y_{sxr} of UNU/ICTP PFF operated under similar conditions for comparison using the CFCM and approximated CM subroutines.

1) *Bank:* Static inductance $L = 110$ nH, $C_0 = 30$ μF, and stray resistance $r = 12$ mΩ.
2) *Tube:* Cathode radius $b = 3.2$ cm, anode radius $a = 0.95$ cm, and anode length $z_0 = 16$ cm.
3) *Operation:* Voltage $V_0 = 14$ kV and pressure $P_0 = 3.0$ torr.

The computed total discharge current waveform is fitted to the measured discharge current by varying model parameters f_m, f_c, f_{mr}, and f_{cr} one by one until the computed waveform agrees with the measured waveform [23]. Current waveform fitting has been successfully obtained using model parameters as follows [23]:

$$f_m = 0.05, \ \ f_c = 0.7, \ \ f_{mr} = 0.2, \ \ f_{cr} = 0.8.$$

These fitted values of the model parameters are then used for the computation of all discharges at various pressures. In Fig. 5, it is observed that the computed discharge current waveform agrees well with the measured current waveform, which covers all the regions of interest from axial to radial phases up to the end of the pinch phase [5], [30], [31]. The same model parameters are used for the current waveform by the Lee model for CFCM and approximated CM methods, which produce the same results, as shown in Fig. 5. Insignificant discrepancy (0.01%–0.24%) in terms of current waveform from start to end in the radial phase around 3.78–3.89 μs is estimated. This affected discrepancy is spotted as the temperature increases from 18 to 200 eV where the ions are just started to be heated and emit as neon SXR. Referring to neon line radiation in (8), the discrepancy of CFCM and approximated CM feasibly influences the outcomes of Y_{sxr}, and there could be more discrepancy as the temperature rises to $\sim$500 eV.

VIII. Results on SXR Yield and Its Parameter Interaction

A series of numerical experiments over the pressure (P_0) range 1.0–4.2 torr is carried out to attain the optimum Y_{sxr} versus P_0 to compare with the measured Y_{sxr} versus P_0 data in [11]. For any shot, whenever the focus pinch temperature is within the range 200–500 eV (2.3×10^6–5.8×10^6 K), the line radiation is counted as neon SXR yield Y_{sxr}. When the pinch temperature is out of this range, the line radiation is not included as neon Y_{sxr} [7], [24].

Comparison of Y_{sxr} versus P_0 via numerical experiments is performed with the CFCM and approximated CM as shown in Fig. 6. It is interesting to note that the neon Y_{sxr} curves show a similar pattern for both the CFCM and approximated CM cases. As the pressure is decreased, the Y_{sxr} keeps increasing until it reaches the optimum values at the same pressure, 3.1 torr. Then, the Y_{sxr} keeps decreasing with lower pressures below their optimum pressures due to the decrease in the density of the pinched radiating plasma, i.e., n_i *pinch* (see Tables I and II).

The results obtained with the CFCM and approximated CM are 3.49 and 3.19 J, respectively. As the pressure goes lower, the percentage of discrepancies becomes diminished, which can be explained by the behavior of pinch ion density n_i *pinch*, as plotted in Fig. 7(a).

According to the temperature range for neon SXR yield, the decrease in n_i *pinch* in the case of CFCM produces higher values than that of the approximated CM. The decrease in n_i *pinch* is also observed as the pressure decreased to the lowest operating pressure. The decrease in n_i *pinch* for the CFCM is estimated around 32% higher than that of the approximated CM at the optimum pressure, i.e., 3.1 torr, which shows substantially high differences between these two cases. The increase in I_{pinch} increases the compression sufficiently so that despite of a drop in ambient number density, the n_i *pinch* is still able to reach a higher value at 3.1 torr. However, the n_i *pinch* does not increase further due to insufficient increase in I_{pinch} below 3.1 torr as shown in Tables I and II for both cases. The other properties of Y_{sxr} as well as the discrepancy can be explained by the parameters included in (8), particularly within the temperature range for neon SXR yield.

Since the values of 200–500 eV (2.3×10^6–5.8×10^6 K) of neon plasma are suitable for neon SXR production, this range is plotted in Fig. 6 to correlate it with the SXR yield Y_{sxr}. It is observed that the temperature at the pinch phase, T_{pinch},

TABLE I
COMPUTED LEE MODEL WITH THE APPROXIMATED CM FOR NEON GAS

P_0 (Torr)	I_{peak} (kA)	I_{pinch} (kA)	T_{pinch} (10^6K)	peak v_s (cm/μs)	r_p (cm)	z_f (cm)	t_{pinch} (ns)	n_i pinch (10^{23}/m^3)	Q_L (J)
4.20	182	90	1.15	16.79	0.09	1.31	11.64	19.97	0.00
4.00	182	94	1.32	17.51	0.08	1.32	10.79	17.63	0.10
3.70	181	99	1.59	18.84	0.07	1.34	9.91	14.56	1.61
3.50	181	103	1.81	19.99	0.07	1.36	9.39	12.66	3.19
3.30	180	103	2.00	21.48	0.06	1.36	8.80	10.64	3.92
3.20	180	108	2.18	22.17	0.06	1.35	8.59	9.65	3.66
3.10	180	110	2.32	22.99	0.07	1.35	8.34	8.78	3.19
2.50	178	119	3.33	25.41	0.08	1.37	8.39	5.42	1.36
2.00	176	125	4.53	26.76	0.09	1.40	8.44	3.84	0.62
1.50	173	129	6.28	29.70	0.09	1.43	7.88	2.68	0.24
1.00	169	130	9.13	34.58	0.10	1.43	6.83	1.73	0.07

TABLE II
COMPUTED LEE MODEL WITH THE CFCM FOR NEON GAS

P_0 (Torr)	I_{peak} (kA)	I_{pinch} (kA)	T_{pinch} (10^6K)	peak v_s (cm/μs)	r_p (cm)	z_f (cm)	t_{pinch} (ns)	n_i pinch (10^{23}/m^3)	Q_L (J)
4.20	182	90	1.16	16.8	0.08	1.29	11.51	13.55	0.81
4.00	182	94	1.33	17.5	0.08	1.31	11.45	11.81	1.36
3.70	181	99	1.61	18.5	0.08	1.36	11.38	12.63	2.77
3.50	181	103	1.82	19.1	0.07	1.38	11.04	13.96	3.90
3.30	180	106	2.06	19.7	0.07	1.39	10.83	13.51	4.15
3.20	180	108	2.19	20.1	0.07	1.40	10.72	12.66	3.92
3.10	180	110	2.32	20.4	0.08	1.39	10.52	11.56	3.49
2.50	178	119	3.30	23.0	0.09	1.38	9.20	6.93	1.33
2.00	176	125	4.29	25.4	0.09	1.39	8.43	4.90	0.58
1.50	173	129	5.70	28.5	0.10	1.40	7.74	3.38	0.22
1.00	169	130	8.40	33.2	0.10	1.42	6.97	2.12	0.06

keeps increasing as the pressure is decreased. This is due to its dependence on the square of the shock speeds, ($T_{\text{pinch}} \propto v_s^2$), and further neon plasma compression [33]. The increase in speed leads to rise in T_{pinch}, which is required for SXR production. The increase in temperature for the CFCM deviates decreasingly from the approximated CM as the pressure is decreased. This is due to the higher v_s of the approximated CM compared with the CFCM, as shown in Tables I and II. At the optimum pressure, temperature with the approximated CM is observed to be 0.9% higher than the CFCM. As the Y_{sxr} is inversely proportional to the T_{pinch}, this could influence the calculation of Y_{sxr} to be deviated largely. However, the T_{pinch} difference at this optimum pressure is considerably small and does not affect much on the optimum Y_{sxr} value. As the pressure is decreased, the percentage of discrepancy for temperatures in both cases increases up to 10%.

It is observed that the suitable T_{pinch} for neon SXR yield is produced for the operating pressure between 1.5 and 3.1 torr for the CFCM. Meanwhile, for the approximated CM, the suitable T_{pinch} for neon SXR yield is produced for the operating pressure between 2.0 and 3.1 torr. This is because below 2.0 torr, the temperature is not suitable for producing neon SXR yield using the approximated CM subroutines. The results show that as the pressure is reduced to 1.5 torr, the neon T_{pinch} for the approximated CM is not anymore considered as the pinch temperature window for neon SXR yield.

In comparison with the approximated CM, the lower v_s corresponds to the lower T_{pinch} values of the CFCM, and thus has a wider range of operating pressures that can be used to obtain the neon SXR yield within the given pinch temperature range, in which this situation could not be achieved by the approximated CM.

The slow compression phase (pinch duration) scales inversely to the square root of the pinch temperature [28]. The pinch duration t_{pinch} slightly reduces for the CFCM as the pinch temperature T_{pinch} increases with decrease in the pressure. Compared with the CFCM, the t_{pinch} for the approximated CM represents almost constant values as the

This article has been accepted for inclusion in a future issue of this journal. Content is final as presented, with the exception of pagination.

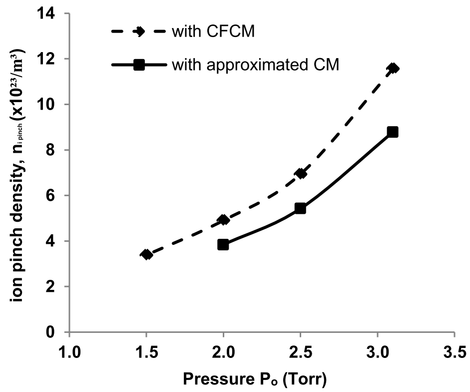

(a)

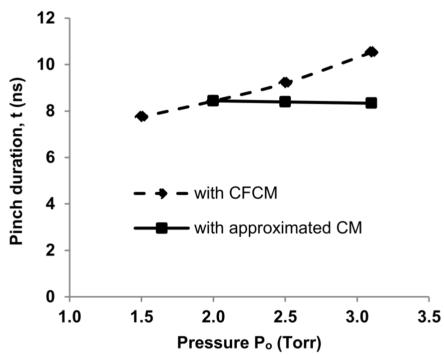

(b)

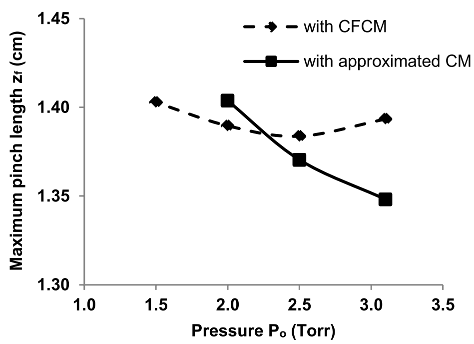

(c)

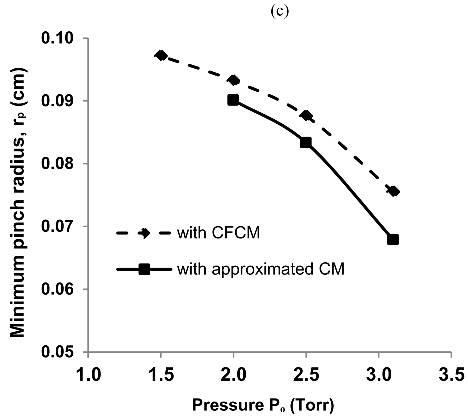

(d)

Fig. 7. (a) Ion pinch density varies with pressure. (b) Pinch duration varies with pressure. (c) Maximum pinch length varies with pressure. (d) Minimum pinch radius varies with pressure.

pressure is decreased. At the optimum pressure, around 20% higher t_{pinch} is observed for the CFCM than that for the approximated CM, as shown in Fig. 7(b), which is considerably high discrepancy compared with other pressures.

In Fig. 7(c), the maximum pinch length, z_f, for CFCM shows an increase in values compared with the approximated CM, particularly at the optimum pressure, 3.1 torr. At this optimum pressure, it is estimated that the pinch length of the CFCM is increased slightly, which is about 3% higher compared with the approximated CM. The z_f increases below the optimum pressure as the pressure is decreased. This is due to the increase in peak v_s, as shown in Tables I and II. However, the z_f parameter only produces minor differences for obtaining the neon Y_{sxr} as it produces small deviations between the CFCM and approximated CM.

Within the range of pinch temperature for neon SXR yield, the minimum radius of the plasma pinch, r_p, during the slow compression phase shows a large difference at a pressure of 3.1 torr, which causes the r_p for the CFCM to produce around 11% higher compared with the approximated CM as the pressure is decreased. Due to insufficient increase in I_{pinch} (see Tables I and II), the r_p does not compress any further below 3.1 torr for both cases.

With the increase in I_{pinch}, the temperature increases, which tends to oppose the severity of the compression during the slow compression phase as the pressure is reduced below 3.1 torr, although the decreased ambient number density tends to work in the opposite direction. The SXR yield depends on the absolute density, which in turn depends on the ambient density and the compression. The smaller the pinch radius ratio (r_p/a), where a is the anode radius, the higher the compression [28]. This shows that the volume that mainly scales as a of the pinch plasma during the slow compression phase also influences the radiation yield.

As shown in Fig. 7(d), the pinch radius r_p is lower for the approximated CM, and it has smaller pinch radius ratio and higher compressibility compared with the CFCM. As the Y_{sxr} depends on the squared of r_p, the values of optimum Y_{sxr} for the CFCM are obtained higher even though compressibility is reduced compared with the approximated CM. In this paper, it is observed that the competing effects of the r_p, t_{pinch}, n_i *pinch*, T_{pinch}, and volume of plasma parameter interaction contribute to the SXR yield for the both cases.

The comparison between the computed and measured data is employed in order to observe the discrepancy among the numerical and experimental results for the Y_{sxr} versus P_0 curves, as shown in Fig. 5. These discrepancies can be explained as follows; in the experimental measurement, uniform source column or hot spots with different aspect ratios (length to radius) affects the dynamics and radiation of the final phase of the focus [11]. While in the numerical experiment, the computation is done for uniform pinch column and other parameters such as radiation duration, bank parameters, tube parameters, operational parameters, and the filled gas, which affect the radiative and quantitative results of the X-ray emission. Although the deviations are existed, the numerical and experimental results are almost in the same magnitude for the pressure below 3.1 torr, compared with the pressure higher than 3.1 torr due to large depletion yield for the computed results. The result with the CFCM shows significantly higher Y_{sxr} corresponding to the pressure and produces optimum Y_{sxr} near the measured result. From Fig. 8, the large depletion or

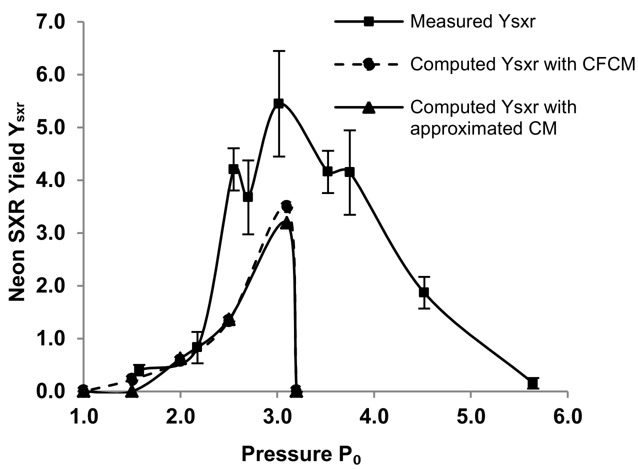

Fig. 8. Experimentally measured Y_{sxr} of UNU/ICTP PFF operated under similar conditions for comparison with numerical experiments with the CFCM and approximated CM.

sharp dropoff in Y_{sxr} is observed at the high-pressure side (3.1–4.2 torr), whereas the temperature is lesser than 200 eV, which is outside the SXR yield temperature range for neon gas.

The comparison of Y_{sxr} versus P_0 between the computed data performed for the approximated CM and CFCM with the measured data is shown in Fig. 8. From the experimental results, it is observed that at the optimum pressure 3.0 torr, an optimum Y_{sxr} of 5.4 ± 1 J [11] is produced. The result of optimum Y_{sxr} for the CFCM is 3.5 J, while that of the approximated CM is 3.2 J.

IX. Conclusion

The neon plasma thermodynamic parameters α, Z_{eff}, and γ are calculated at different temperatures. The close fitting on the Z_{eff} and γ data included in the CFCM for neon is successfully determined by applying fitting in data series using Excel VBA and MATLAB code. Based on the discussed parameter interaction in Y_{sxr}, it is found that with the close fitting of Z_{eff} and γ in the CFCM used in the Lee model, the n_i *pinch* is the key parameter that influences the SXR yield. The n_i *pinch* causes large percentage difference for Y_{sxr} versus pressure for both CFCM and approximated CM cases, especially within the temperature range of neon SXR yield near to the optimum values.

The SXR yield deviations between the computed and experimental results show that the Z_{eff} and γ in the CFCM can be used as more suitable subroutines for the basis of Lee model operation as it increases Y_{sxr} corresponding to the pressure, especially at the optimum Y_{sxr}. The CFCM performance for thermodynamic data gives the potential of numerical experiments to be practically producing more realistic and significant results of SXR yield for neon.

The optimum SXR yield is found to be 3.19 and 3.49 J at the optimum pressure 3.1 torr for the numerical experiment with the approximated CM and CFCM subroutines, respectively, in the Lee model. By applying CFCM subroutines in the Lee model, the SXR radiation yield gives higher values than that of the approximated CM subroutines, which is near to the experimental values. The close fitting on the CM thus shows that it can be contributed to better estimation for further research and gives confidence that the model is sufficiently more realistic in describing the PF dynamics and improving the optimum SXR emission.

Acknowledgment

The authors would like to thank the Institute of Advanced Photonics Science, Nanotechnology Research Alliance and the Physics Department, Universiti Teknologi Malaysia, INTI International University, Malaysia, and the Institute for Plasma Focus Studies, Melbourne, Australia, for collaborative encouragement and assistance in plasma focus research.

References

[1] S. Lee, S. H. Saw, P. Lee, and R. S. Rawat, "Numerical experiments on plasma focus neon soft X-ray scaling," *Plasma Phys. Controlled Fusion*, vol. 51, no. 10, p. 105013, 2009.

[2] I. A. Khan, R. S. Rawat, R. Ahmad, and M. A. K. Shahid, "Post-annealing effect on the structural and mechanical properties of multiphase zirconia films deposited by a plasma focus device," *Chin. Phys. B*, vol. 22, no. 12, p. 127306, 2013.

[3] T. Hussain, R. Ahmad, N. Khalid, Z. A. Umar, and A. Hussnain, "Synthesis of TiN/a-Si_3N_4 thin film by using a Mather type dense plasma focus system," *Chin. Phys. B*, vol. 22, no. 5, p. 55204, 2013.

[4] W. H. Bostick, V. Nardi, and W. Prior, "X-ray fine structure of dense plasma in a co-axial accelerator," *J. Plasma Phys.*, vol. 8, no. 1, pp. 7–20, 1972.

[5] M. Akel, S. Al-Hawat, S. H. Saw, and S. Lee, "Numerical experiments on oxygen soft X-ray emissions from low energy plasma focus using Lee model," *J. Fusion Energy*, vol. 29, no. 3, pp. 223–231, 2010.

[6] M. Akel, S. Al-Hawat, and S. Lee, "Numerical experiments on soft X-ray emission optimization of nitrogen plasma in 3 kJ plasma focus SY-1 using modified Lee model," *J. Fusion Energy*, vol. 28, no. 4, pp. 355–363, 2009.

[7] M. Akel, S. Lee, and S. H. Saw, "Numerical experiments in plasma focus operated in various gases," *IEEE Trans. Plasma Sci.*, vol. 40, no. 12, pp. 3290–3297, Dec. 2012.

[8] S. Lee. (2014). *C1 Introduction File for Corona Calculation*. [Online]. Available: Available: http://www.plasmafocus.net/IPFS/modelpackage/Corona%20Calculations/C1coronaIntroduction.htm

[9] S. Lee. (2014). *Description of Radiative Dense Plasma Focus Computation Package RADPFV5.15 and Downloads—Lee Model Code*. [Online]. Available: http://www.plasmafocus.net/IPFS/modelpackage/File1RADPF.htm

[10] B. Shan, "Comparative study of dynamics and X-ray emission of several plasma focus devices," Ph.D. dissertation, Nat. Inst. Edu., Nanyang Technol. Univ., Singapore, 2000.

[11] M. Liu, "Soft X-rays from compact plasma focus," Ph.D. dissertation, Nat. Inst. Edu., Nanyang Technol. Univ., Singapore, 1996.

[12] S. Al-Hawat and S. Saloum, "Characterization of a 2.8 kJ small plasma focus using a five phase radiative model," *Contrib. Plasma Phys.*, vol. 49, nos. 1–2, pp. 5–14, 2009.

[13] S. Lee and S. H. Saw, "Multi-radiation modelling of the plasma focus," in *Proc. 5th Int. Conf. Frontiers Plasma Phys. Technol.*, Singapore, 2011, pp. 18–22.

[14] L. S. Loh, "Lee's radiative plasma focus model: An improved implementation with auto-tuning of model parameters," Nat. Inst. Edu., Nanyang Technol. Univ., Singapore, 2009.

[15] S. Lee. (2013). *Institute for Plasma Focus Studies*. [Online]. Available: http://www.plasmafocus.net/

[16] S. Lee, "Results of the Internet-based workshop on plasma focus numerical experiments," in *Proc. Int. Workshop Plasma Comput. Appl. (IWPCA)*, 2008, pp. 9–18.

[17] Z. Xu-Tao, "Coronal and local thermodynamic equilibriums in a hollow cathode discharge," *Chin. Phys. Lett.*, vol. 22, no. 5, pp. 1183–1186, 2005.

[18] J. S. Kaastra, F. B. S. Paerels, F. Durret, S. Schindler, and P. Richter, "Thermal radiation processes," *Space Sci. Rev.*, vol. 134, nos. 1–4, pp. 155–190, 2008.

[19] R. W. P. McWhirter, *Plasma Diagnostic Techniques*, R. H. Huddlestone and S. L. Leonard, Eds. New York, NY, USA: Academic, 1965, ch. 5.

[20] A. Burgess, "Dielectronic recombination," in *Proc. 2nd Harvard–Smithsonian Conf. Stellar Atmos.*, 1965, pp. 47–59.

[21] M. J. Seaton, "Radiative recombination of hydrogenic ions," *Monthly Notices Roy. Astron. Soc.*, vol. 119, pp. 81–89, Feb. 1959.

[22] A. Kramida, Y. Ralchenko, and J. Reader. (2013). *National Institute of Standards and Technology (NIST)*. [Online]. Available: http://physics.nist.gov/asd

[23] S. H. Saw, P. C. K. Lee, R. S. Rawat, and P. Lee, "Optimizing UNU/ICTP PFF plasma focus for neon soft X-ray operation," *IEEE Trans. Plasma Sci.*, vol. 37, no. 7, pp. 1276–1282, Jul. 2009.

[24] S. Lee, "Radius ratios of argon pinches," *Austral. J. Phys.*, vol. 36, no. 6, pp. 891–896, 1983.

[25] M. Liu, X. Feng, S. V. Springham, and P. Lee, "Soft X-ray yield measurement in a small plasma focus operated in neon," *IEEE Trans. Plasma Sci.*, vol. 26, no. 2, pp. 135–140, Apr. 1998.

[26] M. Akel, S. Al-Hawat, and S. Lee, "Pinch current and soft X-ray yield limitations by numerical experiments on nitrogen plasma focus," *J. Fusion Energy*, vol. 29, no. 1, pp. 94–99, 2010.

[27] S. H. Saw *et al.*, "The effect of specific heat ratio on neutron yield," *IEEE Trans. Plasma Sci.*, vol. 42, no. 1, pp. 99–104, Jan. 2014.

[28] S. Lee, R. S. Rawat, P. Lee, and S. H. Saw, "Soft X-ray yield from NX2 plasma focus," *J. Appl. Phys.*, vol. 106, no. 2, p. 023309, 2009.

[29] Z. Jiao-Long, Z. Gang, and Y. Jian-Min, "X-ray emission spectra of Ni-like gold ions under coronal plasma condition," *Chin. Phys. Lett.*, vol. 22, no. 8, pp. 1972–1975, 2005.

[30] S. H. Saw and S. Lee, "Scaling laws for plasma focus machines from numerical experiments," *Energy Power Eng.*, vol. 2, no. 1, pp. 65–72, 2010.

[31] S. Lee and S. H. Saw, "Numerical experiments providing new insights into plasma focus fusion devices," *Energies*, vol. 3, no. 4, pp. 711–737, 2010.

[32] M. G. Haines, "A review of the dense Z-pinch," *Plasma Phys. Controlled Fusion*, vol. 53, no. 9, p. 093001, 2011.

[33] M. Akel and S. Lee, "Dependence of plasma focus argon soft X-ray yield on storage energy, total and pinch currents," *J. Fusion Energy*, vol. 31, no. 2, pp. 143–150, 2012.

Natashah Abd Rashid received the B.Sc. degree in pure physics from the Universiti Teknologi Malaysia, Johor Bahru, Malaysia, in 2012, where she is currently pursuing the Ph.D. degree in plasma physics with the Faculty of Science.

Her current research interests include soft X-ray (plasma focus numerical experiment) and learning.

Saiful Najmee Mohamad received the B.Sc. degree in pure physics from the Universiti Teknologi Malaysia, Johor Bahru, Malaysia, in 2012, where he is currently pursuing the Ph.D. degree in plasma physics with the Faculty of Science.

His current research interests include soft X-ray (plasma focus numerical experiment) and learning.

Kashif Tufail Chaudhary received the M.Sc. degree in applied physics from the University of Engineering and Technology, Lahore, Pakistan, in 2008, and the Ph.D. degree in carbon nanomaterials from the Universiti Teknologi Malaysia (UTM), Johor Bahru, Malaysia, in 2014.

He is currently a Visiting Researcher with the Department of Physics, Institute of Advanced Photonics Science, Nanotechnology Research Alliance, UTM. He has a strong grip in experimental physics. His current research interests include nanostructures, plasma physics, and laser-matter incretions.

Sing Lee received the B.Sc. and M.Sc. degrees from the University of Malaya (UM), Kuala Lumpur, Malaysia, in 1964 and 1966, respectively, and the Ph.D. degree from Australian National University, Canberra, ACT, Australia, in 1970.

He was a Professor of Applied Physics and the Head of the Research Groups of Plasma and Pulse Technology and the Department of Physics, UM, and the Head of the Division of Physics and the Academic Group of Natural Sciences with the National Institute of Education, Nanyang Technological University, Singapore. He was an Alexander von Humboldt Fellow with Kernforschunglange, Juelich, Germany, from 1975 to 1976, a Commonwealth Academic Staff Fellow with Imperial College, London, U.K., from 1981 to 1982, a Visiting Professor, and a United Nations University Special Fellow with Flinders University, Bedford Park, SA, Australia, from 1986 to 1987. He is currently the Founding Director of the Institute for Plasma Focus Studies, Melbourne, VIC, Australia, an Adjunct Professor (Hon.) with INTI International University, Nilai, Malaysia, and an Emeritus Professor with UM.

Dr. Lee was the Founder President of the Asian African Association for Plasma Training (AAAPT), an Associate Director of the AAAPT Research and Training Centre with the Institute of Physics, Academia Sinica, Beijing, China, a Far Eastern Representative and the Director of Plasma Physics College with the International Centre for Theoretical Physics, Trieste, Italy, and an Ardent Advocate and Implementer of south-south technology creation and transfer in plasma fusion, laser and pulse technology. He is a Chartered Physicist and fellow of the Institute of Physics, U.K., a Life Fellow and Hon Fellow of the Institute of Physics Malaysia, a Life Fellow of the Singapore Institute of Physics, and the Samahang Pisika ng Pilipinas and Hon Member of the Turkish Science and Research Foundation TUBAV.

Sor Heoh Saw received the B.Sc. (Hons.) and Ph.D. degrees in physics from the University of Malaya, Kuala Lumpur, Malaysia, in 1985 and 1991, respectively, and the M.A. degree in educational management from the University of Nottingham, Nottingham, U.K., in 1997.

She is currently a Professor and the Pro Vice Chancellor for Education Quality and Innovation with INTI International University (IU), Nilai, Malaysia, and the Director of the Centre for Plasma Research. She is a Co-Director of the Institute of Plasma Focus Studies, Melbourne, VIC, Australia, and the Designated Delegate of INTI IU. Her current research interests include plasma physics and innovation in education.

Dr. Saw was conferred the Honorary Membership of Turkish Science and Research Foundation TUBAV in 2009. She was selected as the Vice President of the Asian African Association for Plasma Training from 2012 to 2016.

Jalil Ali received the Ph.D. degree in plasma physics from the Universiti Teknologi Malaysia (UTM), Johor Bahru, Malaysia, in 1990.

He held numerous faculty and research positions, including the Dean/Director, the Bureau of Innovation, and a Consultancy from 1987 to 2010. He was instrumental in establishing and forging University–Industry collaboration in Malaysia. He is currently a Professor of Photonics with the Department of Physics, Institute of Advanced Photonics Science, Nanotechnology Research Alliance, UTM, and a Visiting Professor with King Mongkut's Institute Technology Ladkrabang, Bangkok, Thailand. He is the Head of the Nanophotonics Research Group with UTM, and supervising 20 national/international Ph.D. students as the main supervisor in the field of nanophotonics and plasma focus. His current research interests include photonics, optical solitons, fiber couplers, nanowaveguides, and plasma focus devices.

Dr. Ali is a member of the Optical Society, the International Society for Optics and Photonics, and the Malaysian Institute of Physics. He was a recipient of the Technology Asean Business Review Award for excellence in government delivery services (Innovation) from UTM in 2008. He is an Editorial Member of a number of journals/special issues, such as the *Nanosciences and Nanotechnology: An International Journal*, and an Editorial Board Member of the *Journal of Biosensor and Bioelectronics* of the Special Issue on Biosensors and Bioelectronics On-Chip.